Hindawi
Journal of Nanomaterials
Volume 2022, Article ID 7507729, 11 pages
https://doi.org/10.1155/2022/7507729

Research Article

Electrical Performance Safety Detection of Aramid Casing Based on Molecular Dynamics and Deep Learning Algorithm

Bowen Liu,[1] Fangcheng Lv,[1,2] Xiaozhou Fan,[1] Yueyi Sui,[1] Jiaxue Wang,[1] and Shengdong Yin[3]

[1]*Hebei Provincial Key Laboratory of Power Transmission Equipment Security Defence, North China Electric Power University, Baoding, 071003 Hebei, China*
[2]*State Key Laboratory of Alternate Electrical Power System with Renewable Energy Sources, North China Electric Power University, Beijing 102206, China*
[3]*Ganzhou Longbang Material Technology Co., Ltd., Ganzhou, 341000 Jiangxi, China*

Correspondence should be addressed to Xiaozhou Fan; fxz@ncepu.edu.cn

Received 21 January 2022; Accepted 26 March 2022; Published 11 April 2022

Academic Editor: Palanivel Velmurugan

Transformer bushing is one of the key equipment of transmission system, and its performance directly affects the stability and safety of transmission system. This paper is aimed at studying the safety detection of electrical properties of aramid shells with molecular dynamics and deep learning algorithms. The bushing needs to withstand AC voltage, DC voltage, and polarity reversal voltage during operation. The complexity of operating conditions leads to the improvement of bushing requirements for insulation performance, and bushing accident is a common type of transformer accident, accounting for 30% of the total number of transformer accidents. Therefore, it is necessary to detect the electrical performance and safety of the bushing to ensure the safe and stable operation of the power system. Aramid casing is a kind of casing with many advantages, such as high strength, high tensile breaking force, high stability, and high temperature resistance. Molecular dynamics is helpful to deeply analyze the micro mechanism of various complex phenomena, so as to explain the relationship between material microstructure and macroproperties, so it is very helpful to analyze the structure and properties of aramid casing. Deep learning is an important research direction in the field of machine learning. It can extract important features and simplify casing analysis steps. In this paper, an electrical performance test system of aramid casing is designed. It is proved that the reliability of casing is generally greater than 1 and the reliability is high. The current performance of the bushing is tested. 400 A is a dividing point, and no matter how large the current is, the maximum temperature is no more than 130°, which proves that the current performance of the bushing is stable and the temperature resistance is good. Finally, the radial field strength distribution of bushing capacitor core under different initial moisture content is tested, and it is concluded that the moisture can not be greater than 6%.

1. Introduction

1.1. Background. Bushing is an important part of a transformer. Its safe and reliable operation is related to the operation of the whole power system. Therefore, effective monitoring of transformer bushing has become an important guarantee for the safe and stable operation of power system. For the power system, the main function of the substation is to transmit and distribute power energy. As important key equipment in the substation, the insulation performance of the bushing is related to the overall operation of the transformer. At present, the accidents of power transformer shutdown or damage caused by bushing fault account for 25%~30% of power transformer fault events in the world, and the ratio of bushing fault caused by damp and aging defects accounts for about 40%. However, at present, the traditional diagnosis technology is not sensitive enough to reflect the damp and aging defects of bushing, which is easy to cause the "sick" operation of bushing. Therefore, it is necessary to analyze the electrical performance of the bushing and evaluate the safety of the bushing on this basis.

1.2. Significance. A transformer is very important for the whole power system. It should not only complete voltage exchange but also redistribute and regulate power energy. Its safe and stable long-term operation is the guarantee of power transmission. However, due to the huge workload of power system and complex working environment, there will always be some accidents, many of which are caused by bushing. The bushing capacitor layer is caused by paper insulation breakdown caused by insulation aging and electric field distortion, and its development speed is very fast. At present, the differential protection, overcurrent protection and other devices in transformer body protection can only be started after the bushing is completely broken down, so they can not respond quickly to the bushing breakdown accident. Because the transformer fault can not be completely avoided, whether the electrical performance of bushing can be found and handled early is related to the operation safety of the whole power grid.

1.3. Related Work. Since its emergence, casing has been reused for its practicability and wide application. Its types are diverse, but its uses are similar. So far, many scholars have studied it. Hashemnia et al. introduce detailed simulation and practical analysis to illustrate the influence of bushing fault and transformer oil degradation on transformer FRA characteristics. In this regard, the physical and geometric dimensions of three-phase power transformer are simulated by three-dimensional finite element analysis to simulate the operation of actual transformer. Various bushing faults are simulated on the studied model and oil film, but the deficiency is that the research method is difficult and less practical [1]. Qi et al. designed a bushing model with transparent sheath. The environment of MI in the bushing was simulated by ultrasonic humidifier device and recorded by a digital camera. The parameters such as dielectric loss factor, capacitance, partial discharge (PD), frequency domain response, and moisture content in oil were measured at room temperature. The results show that the low frequency incremental loss factor of 0.001 Hz and the incremental loss factor of 1.2 m can be used to detect the early insulation defects of oil immersed paper bushing, but the research is lack of practicality [2]. Du et al. proposed a scheme for automatic replacement of bushings of DC converter transformers based on a two-dimensional laser profile scanner. This scheme can replace any damaged bushings in the valve chamber without removing other equipment. The initial value of the cylinder fitting algorithm based on the two-dimensional laser profile is also proposed to solve the position of the casing. The algorithm fully considers the characteristics of the laser profile scanner and uses the circle and straight line fitting algorithm to solve the initial value [3]. Srivastava designed a wear test device to measure the sliding temperature and wear amount of aluminum copper metal matrix composite bearing bush in rotating steel shaft. The variation range of weight percentage is 1%, 3%, 5%, 8%, and 10%, respectively. The sample of casing composite material was prepared by powder metallurgy. This study has strong practicability but lacks some detailed design [4]. In order to evaluate the seismic performance of 1100 kV transformer porcelain bushing, Ma et al. carried out finite element analysis and shaking table test on 1100 kV transformer porcelain bushing. The modal frequency, vibration mode, acceleration, strain, and displacement response of EHV casing under matched seismic excitation are obtained. The dynamic characteristics and seismic response of UHV porcelain bushing are predicted by finite element analysis [5]. Liao et al. designed a laboratory oil impregnated paper (OIP) casing model to simulate the damp defects in the oil impregnated paper casing. In addition, Liao et al. also studied the effects of moisture content on dielectric frequency response and polarization and depolarization current (PDC) of oil paper casing model. The results show that in the whole frequency range, the loss factor and capacitance increase with the increase of water content. The quantitative relationship between characteristic parameters, DC conductivity, and water content is established and follows the exponential law. The disadvantage of this experiment is that the possible influencing factors in the actual situation are not considered [6]. In order to evaluate the effectiveness of frequency domain spectroscopy (FDS) in diagnosing the moisture content of oil immersed paper insulating sleeve, Zhang et al. studied the frequency domain dielectric characteristics of oil immersed paper insulating sample and field sleeve. At the same time, the sample and casing with uneven moisture content are analyzed by using the basic principle of interface polarization. The results show that the moisture content will affect the whole frequency band of FDS curve, and the experiment has high requirements for the experimental environment [7].

1.4. Innovation Points. The innovations of this paper are as follows: (1) The electrical performance safety testing method of aramid casing is introduced, and a testing method based on deep learning algorithm and molecular dynamics is proposed. (2) A system is designed and used to detect the safety of aramid casing. The electrical performance indexes of casing are obtained from three aspects of current, electric field, and reliability.

2. Safety Test Method for Electrical Performance of Bushing

2.1. Reliability Solution of Casing. The reliability of casing is an important standard to measure its safety. The reliability of the casing refers to the feasibility of its use. The higher its reliability, the smaller the possibility of damage, the more wear-resistant and compressive, and the longer the corresponding service life. Therefore, here are some methods to measure the reliability of casing.

2.1.1. Probability Distribution of Casing Parameters. According to the statistical data of relevant casing test data, the following formula can be used to represent the pipe size and performance distribution law of casing [8]:

$$f(x) = \frac{1}{\sqrt{2\pi}\sigma_n} \exp\left[-\frac{(x-\mu_n)^2}{2\sigma_n^2}\right], \quad (1)$$

where n is the random variable, μ_n is the mean value of the random variable, and σ_n is the standard deviation of the random variable.

2.1.2. Monte Carlo Method for Casing Reliability Calculation. According to the relevant theoretical knowledge of stress strength interference, assuming that N random variables $X_1, X_2, \cdots, X_n$ are used to describe the functional state of the casing, s is used to represent the load effect on the casing, and R is used to represent the resistance of the casing, the functional function Z of the casing can be expressed as

$$Z = g_X(X_1, X_2..X_n) = R - S. \tag{2}$$

Assuming that the probability density function of casing function Z is known, the casing reliability R can be expressed as

$$R = P(Z > 0) = \int_0^{+\infty} f_z(z)dz. \tag{3}$$

The failure probability of casing is, according to the relevant knowledge of probability theory, as follows:

$$P_s + P_r = 1. \tag{4}$$

If the joint probability density function of n basic random variables $(X_1, X_2, \cdots, X_n)$ in the casing function is known to be $f_x(x_1, x_2, \cdots, x_n)$, the casing reliability R is

$$R = \iiint \cdots f_x(x_1, x_2, \cdots, x_n)dx_1, dx_2, \cdots, dx_n. \tag{5}$$

Assuming that the yield strength of the casing is the fixed value T (the yield strength of the casing refers to the bending resistance of the casing), ignoring the error factors in the casing design, the casing functional state equation can be expressed as [9]

$$Z = g(X) = T - M(y_1, y_2, \cdots, y_m), \tag{6}$$

where X is the random vector $(x_1, x_2, \cdots, x_n)$ composed of all uncertain quantities. According to the above assumptions, then

$$X = Y = (y_1, y_2, \cdots, y_m).. \tag{7}$$

According to the casing reliability solution introduced above, the reliability of casing can be monitored to judge its safety [10].

2.2. Finite Element Calculation Model of Electric Field of Aramid Casing. This model is a model to calculate the electrical performance of the aramid shell. The electric performance of aramid casing is related to the electric field distribution inside and outside the casing. In the casing structure, the field strength of the applied voltage is controlled to prevent the occurrence of discharge phenomena such as breakdown and flashover and to reduce the size and weight of the insulation inside and outside the casing. This section will analyze the potential and electric field distribution of bushing at rated voltage.

2.2.1. Physical Model of Finite Element Calculation of Electric Field. For different types of voltage excitation, there will be corresponding dielectric relaxation time in the dielectric. The relaxation time refers to a dielectric with free charge, and the time required for the movement of free charge is called dielectric relaxation time. Relaxation time is used to express the establishment time of displacement current field and conduction current field under AC and DC voltage excitation, which can be expressed as [7]

$$t = \frac{a}{p}, \tag{8}$$

where t is the relaxation time of the dielectric, a is the dielectric constant of the dielectric, and P is the conductivity of the dielectric. The charge relaxation time at the interface of two different dielectrics is

$$t = \frac{xa_1 + ya_2}{xp_1 + yp_2}. \tag{9}$$

In the above formula, x and y, respectively, represent the insulation thickness of two different dielectrics.

For the total charge relaxation time of materials composed of multimedia, its value is within the range of the minimum and maximum relaxation time of a single medium, which can be expressed as [11]

$$\min\left(\frac{a_1}{p_1}, \cdots, \frac{a_N}{p_N}\right) \le t_e \le \max\left(\frac{a_1}{p_1}, \cdots, \frac{a_N}{p_N}\right). \tag{10}$$

In the above formula, the minimum value refers to the dielectric minimum value. Under AC voltage excitation, the change period T of voltage is much less than the relaxation time of dielectric charge, which can be expressed as

$$T = \frac{2\pi}{\omega} \le t, \tag{11}$$

where t is the period of AC voltage and ω is the angular frequency of AC voltage.

2.2.2. Boundary Type of Electric Field Calculation. When solving the electric field distribution of insulation in bushing with finite element method in static field, first, determine various boundary conditions under the initial state and operating state of bushing without excitation voltage. The following boundary conditions need to be considered in the process of solving steady-state electric field [12]

(1) The first type of boundary condition, also known as Dirichlet boundary condition, is that the potential on the boundary of the solution area is known. For example, the potential of the first screen and the last screen in the insulation in the bushing is known. This condition can be expressed as

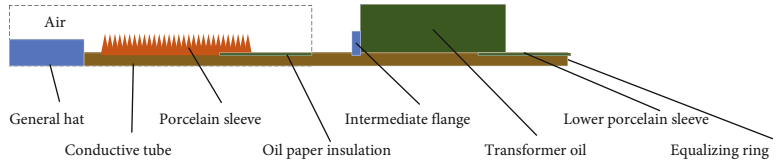

Figure 1: Calculation area of 110 kV bushing electric field.

$$\varphi = \varphi(t) \tag{12}$$

(2) The second type of boundary condition, also known as Neumann condition, is that the normal derivative on the boundary of the solution domain is known, which can be expressed as

$$\frac{\partial \varphi}{\partial n} = 0 \tag{13}$$

2.2.3. Electric Field Distribution Characteristics of Casing. Considering that the casing structure is complex and typical axisymmetric structure, only half of its model area is selected for calculation and analysis. In order to restore the actual running state of the casing and make the calculation results accurate, the air domain and the oil tank can be set as a rectangle, in which the radial length is twice the outer diameter of the casing, the sum of the length of the conservator and the upper porcelain sleeve is the axial length of the air domain, the length of the lower porcelain sleeve is set as the axial length of the oil tank, and the parts below the casing flange are immersed in it. The calculation area of casing electric field shown in Figure 1 [13].

After the casing solution model is established and the relevant material parameters are set, the solution domain is divided into a mesh with a suitable accuracy, and then, the specified type of boundary conditions are applied to the casing. Since the second type of boundary condition software is automatically met, there is no need to manually add it. You only need to manually add the first type of boundary conditions.

2.3. Response Theory of Resistivity Logging in Casing. Casing formation resistivity logging technology is of great significance to oil and gas storage evaluation, production, and various distribution monitoring. It is an important technical means in engineering practice and plays a great role in logging technology. For example, it can be used to determine the remaining oil saturation, identify dead oil and gas reservoirs, evaluate the water flooding of oil reservoirs, monitor fluid saturation, locate oil-water interface, and comprehensively evaluate oil and gas reservoirs in combination with other logging methods. The principle is that in the casing, the formation resistivity measurement is realized by measuring the voltage drop on the casing. To explain in detail, when the current is injected through the tested casing, a large part of the current flows upward or downward along the casing. However, a small part of the injected current still leaks into the surrounding formation, which is the leakage current or called leakage current, which will form a loop with the ground electrode [14, 15].

2.3.1. Electric Field Distribution of Casing Well Point. In a cased well, electrode a is a point power supply with a constant current of I, which is at the shaft position, and its loop electrode and zero reference electrode are at infinity. The origin is point a, as shown in Figure 2. During casing resistivity logging, the electric field can be divided into three areas: near-field area, middle field area, and far-field area. Figure 3 is the distribution diagram of point source electric field [16]

The electric field and current in the formation outside the well are distributed radially along the Z axis of the well, that is, the leakage current, which is related to the formation resistivity. Therefore, casing resistivity logging can be carried out by calculating the second-order potential in the field area. The electric field formula and second-order potential difference formula in the field are given as follows:

$$E(0, Z) \approx \frac{I}{2S_c} e^{-z/\sqrt{Sc/\sigma_f}}. \tag{14}$$

The following is the second-order potential difference formula:

$$\frac{\partial^2 U}{\partial z^2} \approx \frac{I}{2\sqrt{S_c^3}} \sqrt{\sigma_f}.e^{-z/\sqrt{Sc/\sigma_f}}, \tag{15}$$

of which

$$S_c = 2\pi a \bullet \Delta a \bullet \sigma_c. \tag{16}$$

It is the casing conductance. In cased wells, the conductivity generally meets $\sqrt{Sc/\sigma_f} > z$. The formula can be reduced to [17]

$$E(0, Z) \approx \frac{I}{2S_c}, \tag{17}$$

$$\frac{\partial^2 U}{\partial z^2} \approx \frac{I}{2\sqrt{S_c^3}} \sqrt{\sigma_f}. \tag{18}$$

From the above, it is concluded that the electric field in the field is mainly determined by the casing conductance and excitation current. When the casing conductance and excitation current do not change, the electric field does not change. The second-order potential is related to the casing

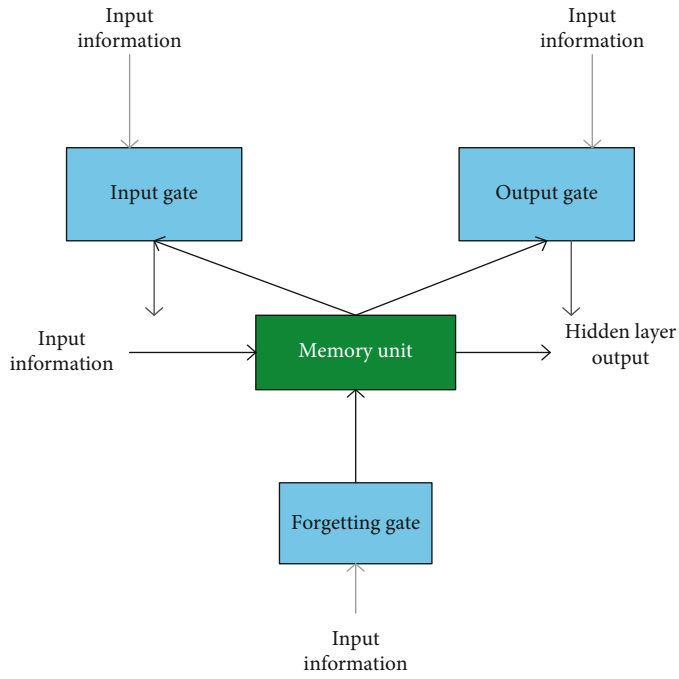

Figure 2: Principle of short-term and long-term memory network.

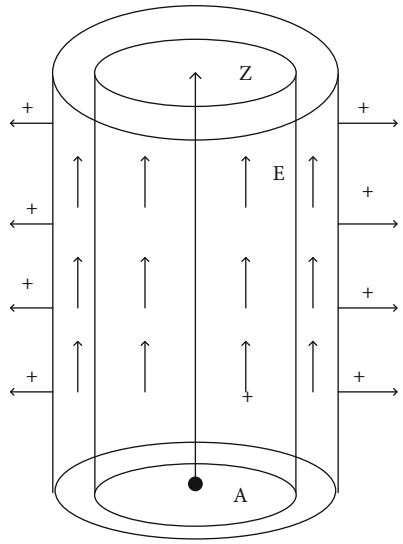

Figure 3: Electric field distribution of casing point source.

conductivity, excitation current, and resistivity outside the casing, so the casing resistivity is an important electrical performance. The resistivity and its impact on the electric field can be obtained through the above algorithm, so as to obtain the electrical performance safety results of the casing [18].

2.4. Casing Safety Assessment Based on Deep Learning. With the arrival of big data boom and the birth of data science and engineering, because deep learning can dig data characteristics and laws in a deeper level, this paper introduces the method of introducing the long-term and short-term memory network in deep learning into casing safety assessment and anomaly early warning.

2.4.1. Establishment of Short-Term and Long-Term Memory Network Model

(1) Short and Long Term Memory Network. Short- and long-term memory networks are a kind of recurrent neural networks. The main difference between the two models is the length of memory maintenance. Due to gradient explosion or gradient disappearance, RNN is not ideal when dealing with nonlinear time series. Therefore, the RNN needs to be improved. The LSTM model is obtained by introducing LSTM element instead of the original hidden layer element. The LSTM unit includes memory unit and three gate structures, namely, input gate, forgetting gate, and output gate. Memory unit and gate structure realize the recording and application of historical information. Its principle is shown in Figure 2 [19].

The basic workflow of LSTM model is as follows:

$$b_t = \sigma(W_{xi}x_t + W_{hi}h_{t-1} + W_{ci}C_{t-1} + d), \tag{19}$$

$$f_t = \sigma\left(W_{xf}x_t + W_{hf}h_{t-1} + W_{cf}C_{t-1} + d\right), \tag{20}$$

$$c_t = f_t C_{t-1} + i_t \tanh\left(W_{xc}x_t + W_{hc}h_{t-1} + d\right), \tag{21}$$

$$o_t = \sigma(W_{xo}x_t + W_{h0}h_{t-1} + W_{c0}C_{t-1} + d), \tag{22}$$

where b_t is the output value of the input gate, f_t is the output value of the forgetting gate, c_t is the status value of memory unit, o_t is the output value of the output gate, d is the offset term, σ is the activation function, generally tan h, and W is the corresponding weight coefficient. The obtained memory unit status value passes through the output gate and multiplied by the output value of the output gate to form the output value of the LSTM unit, so as to realize the long-term memory function of information, as shown in the following [20]:

$$E_t = o_t \tan j(c_t), \tag{23}$$

where E_t is the output value of the hidden layer unit.

2.4.2. Casing Trend Prediction Based on LSTM Model. In trend prediction and safety evaluation based on pipeline monitoring data, the data used are often a large number of historical data obtained from long-term monitoring, and the past data will have an impact on the future monitoring data. Therefore, time correlation needs to be considered. Next, the LSTM model will be used to predict the performance of the pipeline. The main process of casing trend prediction based on LSTM model is as follows: firstly, correlation analysis, that is, listing the factors that may affect casing performance, performing correlation analysis on the relevant factors, obtaining the factors with different influence degrees of equivalent force, determining the number of nodes in the input layer, and determining the number of hidden layers according to the input layer and output layer; Then, classify the performance monitoring data into training set and prediction set, normalize the data, and normalize the training data and test data to eliminate the dimensional influence. When the above steps are completed, the modeling can be carried out, the activation function is selected for training, the relevant parameters are set, and finally, the fitting results are obtained by inverse normalization. Since there are many factors affecting the pipeline monitoring stress, it is necessary to identify the influencing factors with high correlation and use them as input variables, so as to improve the convergence speed and reduce the amount of calculation. The calculation formula is [21]

$$r = \frac{\sum_{i=1}^{n}(x_i - \bar{x})(y_i - \bar{y})}{\sqrt{\sum_{i=1}^{n}(x_i - \bar{x})^2}\sqrt{\sum_{i=1}^{n}(y_i - \bar{y})^2}}, \tag{24}$$

where X is the equivalent stress and Y is the influencing factor. The negative axial strain indicates that the axial strain of the pipeline decreases in practice, which is manifested as compressive strain, while the positive circumferential strain indicates that the circumferential strain of the pipeline increases in practice [22].

3. Electrical Performance and Safety Test of Aramid Casing

3.1. Design of Electrical Safety Performance Test System for Aramid Casing. With the increase of service time, aramid casing will be affected by current, electric field, moisture, pressure, and other factors, resulting in performance degradation, and more seriously, it will directly affect its service life. Therefore, it is necessary to monitor the casing and obtain the changes of casing performance by arranging sensors to monitor stress, current, moisture, and other parameters, so as to judge its safety. It also accumulates basic data for casing safety evaluation and provides data support for casing anomaly early warning.

3.1.1. Casing Performance Detection System. The casing monitoring system is mainly composed of sensor, data collector, and monitoring software. The sensors used in this test include vibrating wire sensor and resistance strain gauge, and the intelligent data collector is selected as the data collector. See Figure 4 for details.

(1) Sensor. Vibrating wire sensors are divided into surface type and embedded type. They are designed with vibrating wire elastic beam structure and are suitable for installation to pipelines, bridges, tunnels, foundation pits, underwater support structures, wharfs, etc. It is fixed on various structural surfaces by pasting, welding, screw installation, drilling with anchor bolts, etc. The vibrating wire sensor will not cause signal attenuation due to wire resistance change and temperature fluctuation. It has the advantages of good stability, easy data recording, strong resistance to external interference, small zero drift, shock resistance, and long service life. Figure 5 is a physical view of the vibrating wire sensor used.

Resistance strain gauge is mainly composed of sensitive grid, substrate, lead, adhesive, and surface layer. It has the advantages of small volume, convenient use, simple operation, and high sensitivity and can reflect the small force after deformation. According to different manufacturing materials, resistance strain gauges are mainly divided into semiconductor and metal. Among them, metal resistance strain gauges have long service life, stable and reliable performance, convenient processing, and many kinds, so they are more convenient to use.

(2) Data Acquisition System. In this experiment, dt85 data collector is selected, which has 16 analog input channels and can record voltage, current and temperature degree, frequency, and other signals. The web-based user interface makes the basic measurement tasks simple and convenient and can be very tolerant. Easily extract the recorded data through the USB cable. The accuracy is shown in Table 1.

The average energy consumption of dt85 data collector is shown in Table 2.

A dt85 intelligent data collector is mainly composed of communication port, power supply, input channel, and calculation channel. The communication port is connected with the computer through three connection modes: network cable, serial port, and USB cable. The input channel includes a digital input channel and an analog input channel. The calculation channel is used for statistical and logical operations

(3) Casing Performance Test Scheme. The overall test scheme is as follows: (1) check whether there is leakage and whether the lifting support, base, and casing are connected reliably before the test. (2) Firstly, monitor the casing performance under normal working conditions; that is, observe and record the data without adjusting the lifting support. (3) The casing shall be reset before each test; that is, the casing shall be restored to the initial state before each test of one

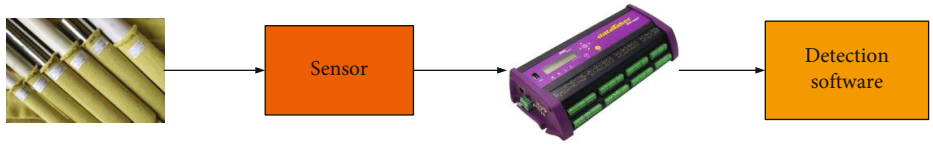

Figure 4: Online detection system

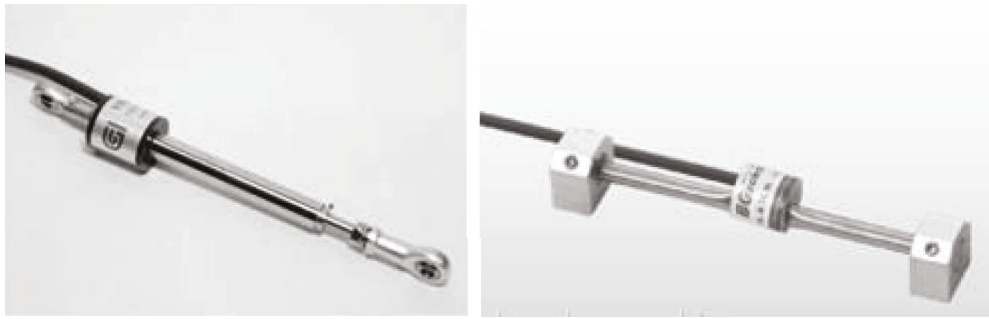

Figure 5: Physical drawing of vibrating wire sensor.

Table 1: Accuracy of dt85 data collector.

	5°C-40°C	-45°C-70°C
DC voltage	0.1%	0.35%
Direct current	0.15%	0.45%
DC resistance	0.1%	0.36%
Frequency	0.1%	0.25%

Table 2: Average energy consumption of dt85 data collector.

Sampling rate	Average energy consumption
1 s	1350 mW
5 s	500 mW
30s	135mW
5 min	70 mW
1 h	60 mW

parameter. (4) Conduct each test; the software automatically records the test time; the vibrating wire sensor and the resistance strain gauge synchronously monitor the safety performance data of the casing and transmit it to the data collector through the cable. (5) After the test, restore the pipe sleeve to the initial state. (6) Check the monitoring data in the dt85 data collector, and import the monitoring data into the computer through the USB cable.

3.2. Realization and Result Analysis of the Experiment. Through the above experimental design, we will carry out practical operation to explore the electrical performance of bushing. The experiment is divided into three parts: the first is to explore the reliability of casing, which is an important index of its safety; the second part is to explore the temperature field distribution of the bushing under different currents, so as to explore the current performance of the bushing; the third part is to explore the influence of the damp state on the casing electric field. Because the use position of the casing is often in the deep soil or dark place, the damp state has become an important influencing factor. Therefore, this part obtains the casing electric field strength value through the change of different damp degrees to explore the casing electric field performance.

3.2.1. Numerical Calculation of Aramid Casing Reliability. Based on the Monte Carlo reliability simulation method in the ANSYS finite element software, due to the complexity of the geometric model, the safety and reliability of the casing are analyzed by fully considering the large uncertainty of the influencing factors of the casing function in the reliability analysis. The random variables in the reliability analysis of this section of casing mainly include mechanical parameters of casing, pressure on inner wall, and temperature load. Table 3 shows the sampling statistical characteristic parameters of main random variables of casing.

According to the calculation and analysis of casing reliability and in combination with the actual situation and the safety situation of casing, the relationship between casing antiextrusion, anti-internal pressure, and safety factor reliability is given. The results are shown in Figure 6.

It can be seen from Figure 6 that when the reliability is between 0.5 and 1.0, the safety factor is greater than 1, when the safety factor increases from 1 to 1.5, the reliability against external extrusion and internal pressure increases from 0.2 and 0.25 to 1, and when the safety factor is greater than 1.5, the reliability is always 1. It can be concluded from the above figure that the reliability of casing is relatively high, which is greater than 1 under normal conditions.

3.2.2. Steady State Distribution of Temperature Field in Aramid Casing. In order to study the influence of different operating loads on the casing temperature distribution, different currents are loaded on the casing conductive rod to analyze the position and size of the hot spot temperature

Table 3: Characteristics of sampling statistics of main parameters.

Parameter	Average value	Standard deviation	Distribution type
External diameter (mm)	177.1	1.67	Normal
Internal diameter (mm)	163.4	1.45	Normal
Yield strength (MPa)	532	1.64	Normal
Temperature (°C)	370	5.98	Normal
Internal pressure (MPa)	55.8	0.67	Normal

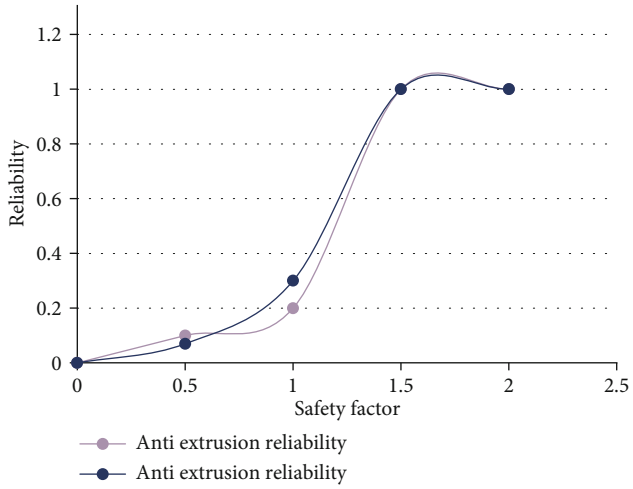

Figure 6: Relationship between safety factor and reliability.

of the conductive rod. The radial and axial paths of the conductive rod are the same as those described in the previous section. The radial temperature distribution characteristics are shown in Figure 7.

It can be seen from the figure that the maximum temperature in the radial direction of the capacitor core appears at the contact between the oil impregnated paper and the conductive rod. When the loading current is lower than 400 A, the internal and external temperature of the capacitor core has no obvious downward trend. When the current is above 400 A, the internal and external temperature of the capacitor core decreases significantly. This is because when the loading current is small, the Joule heating temperature caused by the current is lower than the temperature of the hot oil in the transformer oil tank. At this time, the hot oil in the oil tank transfers heat to the bushing through heat conduction and heat convection. When the loading current is large, the Joule heating caused by the current is much greater than the temperature of the hot oil in the oil tank, and the temperature of the capacitor core gradually decreases from inside to outside.

Next, Figure 8 shows the steady-state distribution parameters of casing axial temperature field under different currents.

It can be seen from Figure 8 that the hot spot temperature in the casing appears at a point of the conductive rod in the lower half of the casing. With the increase of the loading current, the position of the hot spot temperature increases axially upward.

In conclusion, the maximum radial temperature field is 119° and the maximum axial temperature field is 130°, and then, the temperature will decrease with the depth of the capacitor core. Moreover, the current of 400 A is a dividing point. Under different operating loads, the temperature inside and outside the capacitor core is relatively consistent in the radial direction when the loading current is lower than 400 A; when the current is higher than 400 A, the temperature of the capacitor core decreases significantly from inside to outside. Axially, the hot spot temperature of the casing appears at a point of the conductive rod in the lower half of the casing. With the increase of the loading current, the position of the hot spot temperature increases upward. This proves that the current performance of the bushing is stable and the temperature resistance is good.

3.2.3. Influence of Damp State on Electric Field Distribution of Casing. Since the capacitance core shows certain water distribution characteristics in the axial and radial directions under different external influencing factors, the capacitance core is divided into finite solution regions according to the axial and radial water changes of each insulating layer in this section, and the water mass fraction of each solution domain is obtained by simulation. There is a relevant corresponding relationship between the water content and the relative dielectric constant. At this time, the ambient temperature of the capacitor core is 70°C. The electric field distribution of oil immersed bushing in damp state can be obtained by knowing the distribution of relative dielectric constant of capacitor core in different damp states.

(1) Influence of Damp Time on Electric Field Distribution. The finite element calculation of casing radial electric field under uneven water distribution is carried out. The moisture content of the initial invasion of the bushing is set to be 0.5%, 3%, 5%, and 6%, respectively, and the operating temperature of the bushing is 70°C. The moisture distribution state of the capacitor core at the 100th day is selected as the research object. According to the moisture distribution characteristics of the capacitor core, the capacitor core is divided into 42 nonoverlapping calculation areas, and the difference of moisture content between adjacent areas is 0.01%-0.1%. By substituting the relative dielectric constant ‰r corresponding to different moisture contents into the material properties of relevant calculation areas, the radial field strength of bushing under different initial intrusion moisture contents can be obtained. As shown in Figure 9, the radial field strength distribution diagram of bushing capacitor core is shown, and the radial path of the outermost layer of the core is selected.

When the capacitor core is dry as a whole, the radial field strength in the capacitor core presents a U-shaped distribution from inside to outside. The field strength at the first screen and the last screen is the largest, up to 2.3 kV/mm, and the field strength at a certain layer of electrode plate in

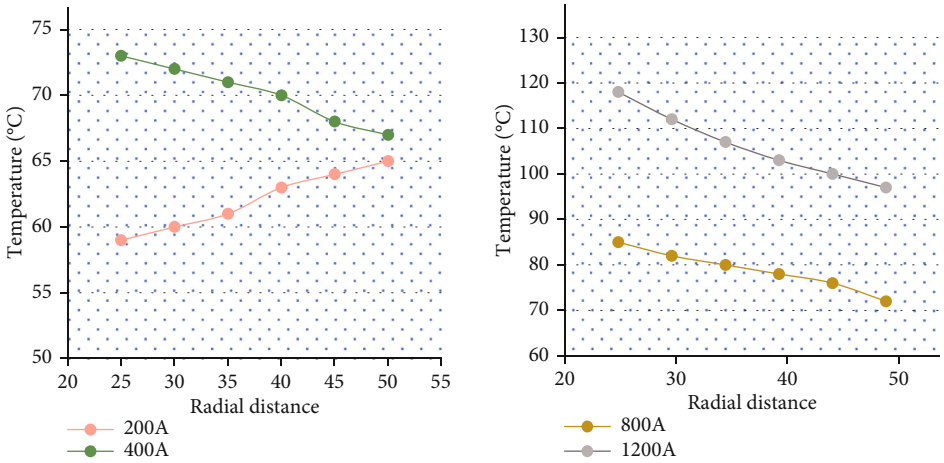

Figure 7: Steady state distribution of casing radial temperature field under different currents.

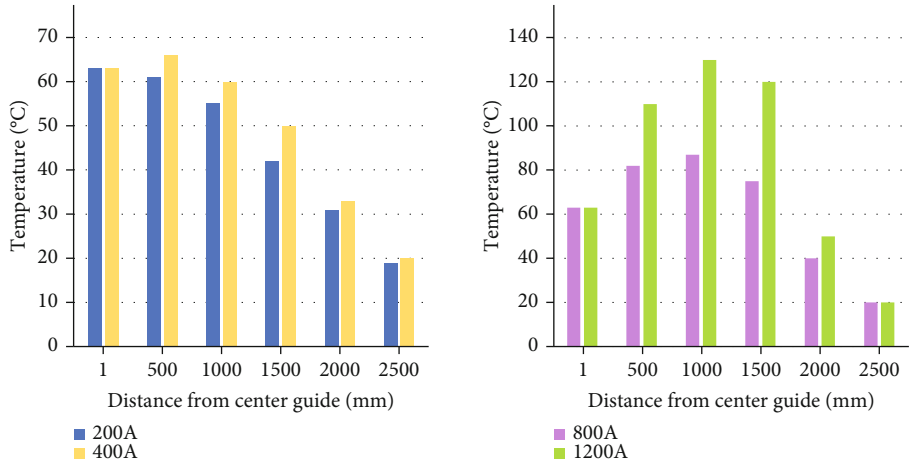

Figure 8: Steady state distribution of axial temperature field of casing under different currents.

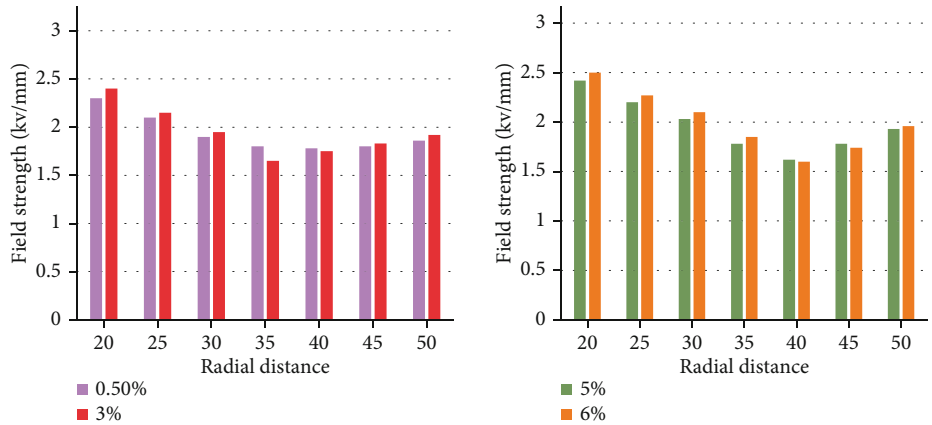

Figure 9: Radial field strength distribution of bushing capacitor core under different initial moisture content intrusion.

the middle is the smallest, 1.78 kV/mm. When there is water intrusion at the leakage, the uneven distribution of water in the capacitor core is remarkable. At this time, the radial field strength at the first screen of the capacitor increases slightly, and the minimum radial field strength in the middle layer decreases obviously. With the increase of water content at the intrusion, the minimum radial field strength will decrease accordingly, and the radial field strength at the

outermost layer of the capacitor core remains basically unchanged. At this time, the field intensity distribution in the capacitor core is nearly V-shaped. It can be seen that when there is water intrusion in the electric core, the uneven distribution of field strength of the capacitor core intensifies, which shows that the maximum field strength increases relative to the dry state, the minimum field strength decreases relative to the dry state, and partial discharge occurs when the bushing runs in this state for a long time.

It can be seen that regardless of the degree of moisture, the radial field strength distribution trend of the capacitor core does not change, which is a U-shaped distribution from inside to outside, but the field strength will generally increase with the increase of the degree of moisture. The moisture content at the intrusion point is 6%, and the overall temperature of the capacitor core is greater than the withstand temperature of the insulating paper. When the moisture content at the invasion point is small, the invasion time has little contribution to the overall temperature rise of the casing. When the moisture content at the intrusion point is large, the capacitor core also has a large temperature rise in a short time, and the capacitor core will soon reach the insulation withstand temperature.

4. Discussion

Bushing is the key component of power equipment such as a power transformer and circuit breaker. Its reliable operation plays an important role in the safety and stability of power system. As the link between the internal insulation and the external insulation system, the bushing not only bears the internal high electric field force, mechanical force, and thermal stress but also is affected by the external environment, such as pollution and moisture, so it is very prone to insulation failure. However, the failure of the bushing is often difficult to find. Once the bushing fails, it will damage the electrical equipment connected to it and may threaten the personal safety of on-site staff. Therefore, in order to find faults in time and take effective measures to avoid large power system accidents and ensure the safe and reliable operation of transformers and other equipment connected with them, it is of great significance to evaluate the power performance of bushings reliably and accurately.

5. Conclusions

This paper introduces the test algorithm for the electrical performance safety evaluation of aramid casing, including the evaluation algorithm based on deep learning, and designs experiments to evaluate the electrical performance safety of aramid casing. The details are as follows: (1) the reliability calculation method of casing and the physical model of finite element calculation are introduced. (2) This paper introduces the long-term and short-term memory network in deep learning and designs the method of measuring casing safety based on LSTM model. (3) A system for measuring casing performance is designed, including its system design and scheme. (3) The experiment realizes the reliability test of aramid casing and comes to the conclusion that its reliability is generally greater than 1, with high reliability. (4) The experiment realizes the steady-state distribution of radial and axial temperature field of bushing under different currents. It is concluded that the maximum value of radial temperature field is 119°, the maximum value of axial temperature field is 130°, and then the temperature will decrease with the depth of capacitor core. This proves that the current performance of the bushing is stable and the temperature resistance is good. (5) The radial field strength distribution of bushing capacitor core under different initial moisture content invasion is tested. It is concluded that the moisture content at the entrance and exit point is 6%, and the overall temperature of capacitor core is greater than the withstand temperature of insulating paper.

Data Availability

The data that support the findings of this study are available from the corresponding author upon reasonable request.

Conflicts of Interest

The authors declare that they have no conflicts of interest.

Acknowledgments

This paper is supported by the National Natural Science Foundation of China (51777076).

References

[1] N. Hashemnia, A. Abu-Siada, and S. Islam, "Detection of power transformer bushing faults and oil degradation using frequency response analysis," *IEEE Transactions on Dielectrics and Electrical Insulation*, vol. 23, no. 1, pp. 222–229, 2016.

[2] B. Qi, Q. Dai, C. Li, Z. Zeng, M. Fu, and R. Zhuo, "The mechanism and diagnosis of insulation deterioration caused by moisture ingress into oil-impregnated paper bushing," *Energies*, vol. 11, no. 6, p. 1496, 2018.

[3] X. Du, A. Xiao, and H. Yue, "Automated replacement scheme of DC transformer bushing based on laser scanning profile: design and experiment," *Electric Power Systems Research*, vol. 192, no. 4, article 106967, 2021.

[4] V, K, Srivastava, "Wear behaviour of alumina filled Al-Cu metal-matrix composite bushing with rotating steel shaft. International," *Journal of Composite Materials*, vol. 6, no. 5, pp. 159–166, 2016.

[5] M. A. Guoliang, L. I. A. O. Defang, H. E. Chang, and X. I. E. Qiang, "Seismic performance of a 1100 kV transformer bushing," *Gaodianya Jishu/High Voltage Engineering*, vol. 43, no. 6, pp. 2033–2041, 2017.

[6] R. Liao, Y. Du, L. Yang, and J. Gao, "Quantitative diagnosis of moisture content in oil-paper condenser bushing insulation based on frequency domain spectroscopy and polarisation and depolarisation current," *IET Generation Transmission & Distribution*, vol. 11, no. 6, pp. 1420–1426, 2017.

[7] D. Zhang, H. Zhao, H. Yun et al., "Study on FDS characteristics of oil-immersed paper insulation bushing under non-uniform moisture content," *IET Science, Measurement and Technology*, vol. 12, no. 5, pp. 691–697, 2018.

[8] Q. Liu, J. D. Yan, L. Hao, B. Zhang, and S. Liu, "Charge transport and accumulation around a spancer insulator for application in HVDC wall bushing," *IEEE Transactions on Dielectrics and Electrical Insulation*, vol. 25, no. 1, pp. 281–293, 2018.

[9] Q. B. Dai Quanmin and Z. Ran, "Discharge process and characteristics of the poor impregnated defect of capacitor core in oil-immigrated paper bushing," *Diangong Jishu Xuebao/ Transactions of China Electrotechnical Society*, vol. 32, no. 7, pp. 181–189, 2017.

[10] C. C. Wang and J. P. Hung, "Theoretical and bifurcation analysis of a flexible rotor supported by gas-lubricated bearing system with porous bushing," *Journal of Vibroengineering*, vol. 18, no. 3, pp. 1934–1940, 2016.

[11] M. A. Guoliang, Z. H. U. Ruiyuan, and X. I. E. Qiang, "Shake table testing of a base-isolated transformer bushing system," *High Voltage Engineering*, vol. 43, no. 4, pp. 1317–1325, 2017.

[12] X. Luo, W. Hu, and T. Xu, "Air gap flashover characteristics and selection of gap distances for ±1100 kV DC U-shaped wall bushing," *High Voltage Engineering*, vol. 43, no. 3, pp. 946–952, 2017.

[13] Z. Wei, X. Zhu, X. Chen, and L. Zhang, "Fatigue life analysis of rear bushing of automobile control arm on bench test," *Journal of Mechanical Engineering*, vol. 52, no. 12, pp. 81–89, 2016.

[14] O. Aljohani and A. Abu-Siada, "Application of digital image processing to detect transformer bushing faults and oil degradation using FRA polar plot signature," *IEEE Transactions on Dielectrics & Electrical Insulation*, vol. 24, no. 1, pp. 428–436, 2017.

[15] L. Cao, F. Sadeghi, and L. E. Stacke, "An explicit finite-element model to investigate the effects of elastomeric bushing on bearing dynamics," *Journal of Tribology*, vol. 138, no. 3, article 031104, 2016.

[16] H. H. Lee, "Development of in-line machining quality prediction system based on inner-circle precision measurement for reducing bushing machining defect," *Journal of The Korean Society of Manufacturing Technology Engineers*, vol. 30, no. 3, pp. 239–243, 2021.

[17] Y. Haryono, A. Harianto, and E. Rinawiyanti, "Optimization of boring process parameters in manufacturing of polyacetal bushing using high speed steel," *E3S Web of Conferences*, vol. 130, no. 3–4, p. 01031, 2019.

[18] D. Duerr, "Erratum for Lifting lug with pinhole bushing by David Duerr," *Practice Periodical on Structural Design and Construction*, vol. 24, no. 4, p. 08219001, 2019.

[19] J. Q. Chen, "Fault prediction of a transformer bushing based on entropy weight TOPSIS and gray theory," *Computing in Science & Engineering*, vol. 21, no. 6, pp. 55–62, 2019.

[20] Z. Li, W. Li, H. Tang, P. Jia, and S. Zhang, "Insulation condition assessment for power transformer bushing based on set pair analysis and comprehensive weights," *Gaoya Dianqi/High Voltage Apparatus*, vol. 54, no. 3, pp. 115–121, 2018.

[21] Z. Demir and O. Adiyaman, "Investigate the bushing shape in Mould supported thermal friction drilling," *International Journal of Research-GRANTHAALAYAH*, vol. 6, no. 8, pp. 226–237, 2018.

[22] G. L. Ma, Q. Xie, and A. S. Whittaker, "Physical and numerical simulations of the seismic response of a 1, 100 kV power transformer bushing," *Earthquake Spectra*, vol. 34, no. 3, pp. 1515–1541, 2018.